universe

IMPACT FACTOR 2.6

CITESCORE 5.2

Article

Galactic Cosmic Ray Interaction with the Perseus Giant Molecular Cloud Using Geant4 Monte Carlo Simulation

Luan Torres and Luiz Augusto Stuani Pereira

Special Issue

Ultra-High Energy Cosmic Rays: Past, Present and Future

Edited by

Dr. Dmitriy Kostunin and Dr. Vladimir Lenok

MDPI

https://doi.org/10.3390/universe11070218

universe

MDPI

Article

Galactic Cosmic Ray Interaction with the Perseus Giant Molecular Cloud Using Geant4 Monte Carlo Simulation

Luan Torres [1,*,†] and Luiz Augusto Stuani Pereira [1,2,*,†]

[1] Unidade Acadêmica de Física, Universidade Federal de Campina Grande (UAF-UFCG), R. Aprígio Veloso, 882, Campina Grande 58429-900, PB, Brazil
[2] Instituto de Física, Universidade de São Paulo (IFUSP), R. do Matão, 1371, São Paulo 05508-090, SP, Brazil
* Correspondence: luan.castro@estudante.ufcg.edu.br (L.T.); luizstuani@uaf.ufcg.edu.br (L.A.S.P.)
† These authors contributed equally to this work.

Abstract

Galactic cosmic rays (GCRs), composed of protons and atomic nuclei, are accelerated in sources such as supernova remnants and pulsar wind nebulae, reaching energies up to the PeV range. As they propagate through the interstellar medium, their interactions with dense regions like molecular clouds produce secondary particles, including gamma-rays and neutrinos. In this study, we use the Geant4 Monte Carlo toolkit to simulate secondary particle production from GCR interactions within the Perseus molecular cloud, a nearby star-forming region. Our model incorporates realistic cloud composition, a wide range of incidence angles, and both hadronic and electromagnetic processes across a broad energy spectrum. The results highlight molecular clouds as significant sites of multi-messenger emissions and contribute to understanding the propagation of GCRs and the origin of diffuse gamma-ray and neutrino backgrounds in the Galaxy.

Keywords: galactic cosmic rays; Perseus molecular cloud; cosmic secondary particles

Academic Editors: Dmitriy Kostunin and Vladimir Lenok

Received: 9 May 2025
Revised: 25 June 2025
Accepted: 30 June 2025
Published: 2 July 2025

Citation: Torres, L.; Stuani Pereira, L.A. Galactic Cosmic Ray Interaction with the Perseus Giant Molecular Cloud Using Geant4 Monte Carlo Simulation. *Universe* **2025**, *11*, 218. https://doi.org/10.3390/universe11070218

1. Introduction

Cosmic rays (CRs) are high-energy relativistic particles, primarily protons and ions, that permeate our Galaxy. Their energy spectrum ranges from a few MeV up to 10^{20} eV, with a Galactic component contributing at least up to $\sim 3 \times 10^{15}$ eV (3 PeV) [1]. These particles are fundamental to numerous phenomena in astrophysics, not only influencing the chemistry and dynamics of cosmic structures, but also contributing to the ionization of interstellar and cosmic feedback mechanisms in star formation. Supernova remnants (SNRs) are among the most promising candidates for Galactic CR (GCR) sources. They not only provide the necessary energy budget to sustain the observed GCR population, but also create ideal conditions for first-order Fermi acceleration, making them efficient CR accelerators [2]. Galactic molecular clouds serve as valuable tracers of various CR interactions and processes within the Galaxy [3]. Subrelativistic CRs can be studied through potential emissions such as the de-excitation iron 6.4 keV line or by analyzing hydrogen ionization rates within these clouds [4–8]. Meanwhile, insights into relativistic CRs can be obtained by observing gamma-ray emissions from molecular clouds [9–13].

The interstellar medium (ISM) is a complex, multi-phase environment, where cold, dense molecular clouds (MCs) coexist with hot, diffuse gas in approximate pressure equilibrium. MCs form as the hot ISM gas cools and collapses under gravity, reaching typical densities of $\sim 10^2$ cm^{-3}, temperatures around 10 K, and sizes ranging from a few to several

tens of parsecs. These clouds are threaded by magnetic fields of a few μG, likely dragged in from the ISM during collapse, resulting in a characteristic "pinching" effect on the field orientation [14]. The interaction of CRs with MCs initiates a range of physical and physicochemical transformations, from energy deposition that heats the system to particle cascades and molecular dissociation, ultimately leading to the formation of new chemical species [5,15]. The secondary particles generated in these interactions, such as protons, neutrons, muons, pions, electrons, and photons, engage with the surrounding medium through various processes, transferring energy both directly and indirectly. Significant efforts have been dedicated to understanding how energy is deposited across different regions of the MC by CR-induced particles and its role in the cloud's thermal balance.

Perseus MC is an exemplary region for the study of GCR interactions due to its proximity and richness in star formation activity. Located in the constellation Perseus at a distance of approximately 956 to 1047 light-years (293 to 321 pc) from Earth, reflecting the cloud's physical extent along the line of sight, the Perseus molecular cloud hosts the formation of both low- and high-mass stars, making it an ideal target for studying how Galactic cosmic rays interact with dense gas and dust. The cloud structure, characterized by regions of varied density and temperature, serves as both a barrier and a catalyst for cosmic ray particles. Zhang et al. [16] contributed substantially to our understanding of the composition of the Perseus MC through observational data derived from various wavelengths. His work has identified essential constituents such as H_2, CO, and other complex organic molecules, which are crucial for modeling chemical reactions in high-density environments. This molecular diversity can improve or inhibit cosmic ray interactions, thus affecting the general spectrum of cosmic rays observed near the cloud. Yang et al. [11] provided evidence suggesting that Perseus MC acts as a source of secondary cosmic rays generated through interactions between high-energy particles and the dense molecular gas. Ge & Liu [17] further elaborated on this phenomenon, detailing how the proximity of SNRs adjacent to the cloud can lead to increased cosmic-ray escape rates, thus contributing to the general population of cosmic rays that cross the ISM.

Monte Carlo simulations of CRs have been widely employed to study energy transfer processes in the ISM and other astrophysical environments. For example, Helling et al. [18] investigated how CRs drive ionization and discharge processes in the atmospheres of brown dwarfs and exoplanets. However, many of these models primarily consider CR energy input from protons or proton–alpha particle interactions, typically governed by interaction cross-sections [19]. A critical limitation of most models is their exclusion of cascade particles and the complex energy distribution associated with secondary particle production and release. In this work, we investigate the energy deposited by cascade particles and the distribution of secondary particles within the Perseus molecular cloud, which has an approximate size of 3.16×10^7 au (∼500 lt-yr ∼153 pc) and a mass exceeding 10^4 $M_\odot$. Following the geometry assumptions adopted in [20], we model the cloud as a sphere to enable tractable simulations while acknowledging that this simplification may affect the estimated density due to the cloud's extended structure. The Geant4 library has a well-documented set of models that allow us to simulate cosmic ray interactions within the MC of Perseus [20]. Geant4 is a comprehensive software toolkit designed to simulate particle passage through matter, allowing the exploration of complex interaction processes, including energy transfer and secondary particle production [21].

Given this context, the present work provides a systematic simulation study of galactic cosmic ray interactions with the Perseus molecular cloud using the Geant4 Monte Carlo toolkit. We investigate the energy deposition and secondary particle production by various primary species (electrons, protons, alpha particles, carbon, and iron nuclei) across a wide energy range (10 GeV to 100 TeV) and multiple incidence angles (1° to 80°). The cloud is

modeled as a spherically symmetric structure composed of concentric layers with astrophysically motivated density and composition. By tracking the interaction of each primary and the resulting secondaries, we characterize the spatial distribution of energy deposition and the emergent particle spectra. The results presented in this work aim to enhance our understanding of energy transfer mechanisms in dense interstellar media and contribute to the development of more accurate models of particle transport and secondary particle generation in molecular clouds. In particular, by systematically evaluating the angular and species dependence of energy deposition and secondary yields, this study provides benchmark data that can support the calibration of propagation codes and inform the interpretation of gamma-ray and neutrino emissions from nearby star-forming regions such as Perseus.

Section 2 outlines the theoretical framework and computational methodologies adopted in this study, with particular emphasis on the implementation of the Geant4 Monte Carlo simulation toolkit. This includes detailed descriptions of the nuclear cascade processes modeled, as well as the geometrical configurations and parameterizations utilized throughout the simulations. The primary findings and their interpretation are presented in Sections 3 and 4, where the implications of the results are critically discussed. A summary and conclusions are presented in Section 5.

2. Methodology

We utilized the Monte Carlo toolkit Geant4 v10.1 [22,23] to model the geometry, composition, and cosmic radiation transport within the Perseus giant molecular cloud MC. The following sections outline the key aspects of our simulations, including the MC's structural and compositional modeling, the generation of incident cosmic radiation, and the relevant Geant4 physics implemented in this study. This approach enables us to explore how cosmic ray energy transfer depends on primary composition, energy, and incidence angle, parameters that directly influence gamma-ray and neutrino production in star-forming regions. By providing controlled, high-resolution simulations across these dimensions, we aim to generate benchmark data relevant for the interpretation of multi-messenger astrophysical observations.

2.1. Geometry and Composition Modeling

The geometry and composition of the Perseus MC were constructed based on the work of Pazianotto et al. [20], in which the geometry of the MC is adopted as a spherical configuration subdivided into 6 concentric layers with varying radii. The density within the MC follows a radial profile proportional to $r^{-1.2}$, where r represents the mean radius of each layer. The power-law index of -1.2 reflects an average value consistent with observed MC density distributions [24]. To implement this profile within the Geant4 framework, the cloud is divided into concentric spherical shells with stratified densities that approximate the continuous radial variation. This discretization approach balances computational efficiency with physical realism. The Perseus MC has a diameter of approximately $\sim$153.20 pc and its total mass is approximately 10^4 $M_\odot$ [25].

The chemical composition of the Perseus molecular cloud in our model is based on astrophysical observations and tailored to capture its role as a dense target for cosmic ray interactions. We represent the cloud as a mixture of molecular hydrogen (H_2), helium (He), and carbon, accounting, respectively, for 90%, 9%, and 1% of the atomic number abundance. This composition reflects the dominance of H_2 in dense regions [26] and includes helium at its typical cosmic abundance. Although the carbon abundance is enhanced relative to the average interstellar medium ($\sim$0.17%), we adopt a 1% value to ensure effective modeling of energy deposition processes involving dust grains, which significantly affect

secondary particle cascades. This enhancement does not alter the global realism of the model but allows us to explore the influence of dust-related hadronic and electromagnetic processes, which are otherwise underrepresented in standard Geant4 configurations. Each spherical shell of the cloud maintains this composition, modulated locally by density and temperature gradients derived from observational constraints. The presence of dust plays a crucial role in shielding molecules from photodissociation and in facilitating the formation of complex molecules [27].

The temperature of gas and dust in molecular clouds is an important parameter for understanding the physical conditions and processes within these interstellar environments, including the influence of cosmic rays as a primary ionizing agent. In the Perseus molecular cloud, gas temperatures primarily correspond to the denser regions, ranging from approximately 60 K to 75 K depending on local density, composition, and location within the cloud. Dust temperatures have been reported to vary between 16 K and 22 K [25,26,28,29]. These temperature values are taken from previous observational and modeling studies to provide environmental context; however, they are not directly used as input parameters in our Geant4 simulations, which rely on explicitly specified gas densities. Table 1 summarizes the densities along with the gas and dust temperatures considered for each layer of the molecular cloud.

Table 1. Properties of the Cloud Spherical Layers Adopted in the Model.

Layers	Outer and Inner Radius (pc)	H_2	He	C	Density (g/cm^3)	Gas and Dust Temperature (K)
Layer 1	153.2–127.7	90%	9%	1%	1.65×10^{-23}	75 & 22.0
Layer 2	127.7–102.2	90%	9%	1%	2.07×10^{-22}	72 & 20.8
Layer 3	102.2–76.6	90%	9%	1%	2.48×10^{-22}	69 & 19.6
Layer 4	76.6–51.1	90%	9%	1%	2.89×10^{-22}	66 & 18.4
Layer 5	51.1–25.6	90%	9%	1%	3.30×10^{-22}	63 & 17.2
Layer 6	25.6–0.0	90%	9%	1%	3.98×10^{-22}	60 & 16.0

2.2. Particle Spectra and Incidence Direction

The primary cosmic radiation used in the simulations was derived from observational data obtained by different space missions (AMS-02[1], CALET[2], *Fermi*-LAT[3], CREAM[4], PAMELA, TRACER[5], DAMPE[6] e BESS-Polar II), which are available in the Cosmic Ray DataBase (CRDB) [30,31], a centralized repository dedicated to charged cosmic ray measurements. CRDB provides a user-friendly interface for querying and retrieving data based on particle species, energy ranges, and specific experiments. It encompasses measurements for electrons, protons, and various nuclei, including helium, carbon, and iron, which are pertinent to our model. The database includes detailed information on fluxes, energy spectra, and associated uncertainties, facilitating accurate and comprehensive simulations. For instance, AMS-02 provides precise flux measurements of cosmic ray protons, helium, and heavier nuclei over a wide energy range, while CALET and DAMPE offer high-resolution data on electron and gamma-ray spectra. Similarly, CREAM and TRACER contribute valuable information on the composition and energy spectra of heavier nuclei.

Figure 1 shows the charged particle spectra used in the simulations. Although the displayed primary cosmic ray spectra span a wide energy range from 100 MeV to 100 TeV, in the Geant4 simulations, we restricted the injection range to 10 GeV–100 TeV. This lower energy threshold was adopted for both physical and computational reasons. First, cosmic rays with energies below 10 GeV are strongly affected by solar modulation and magnetic shielding, making their flux and penetration depth in molecular clouds highly uncertain. Second, low-energy primaries deposit energy over very short distances, leading to localized

interactions with minimal production of detectable secondary particles escaping the cloud. From a computational standpoint, simulating such low-energy events significantly increases processing time without substantially contributing to the emergent high-energy particle spectra of interest. Therefore, focusing on the 10 GeV to 100 TeV range provides a more realistic and efficient representation of the high-energy processes relevant for interpreting gamma-ray and neutrino observations from dense astrophysical environments.

To investigate the impact of cosmic ray injection angle on particle propagation and energy deposition within the molecular cloud, we implemented a controlled variation of the angle θ, defined as the angle between the direction of the incoming cosmic ray and the longitudinal axis of the cylindrical cloud. The simulations cover a range of θ values to emulate different entry geometries, from nearly parallel to highly inclined trajectories. This setup allows us to assess how angular incidence influences the spatial distribution of deposited energy inside the cloud. Understanding this angular dependence is essential for interpreting potential anisotropies in secondary emission signatures, such as gamma-rays and neutrinos. Figure 2 illustrates the injection geometry, showing how variations in θ affect primary particle trajectories and the development of secondary cascades, a critical aspect discussed in Section 3.1.

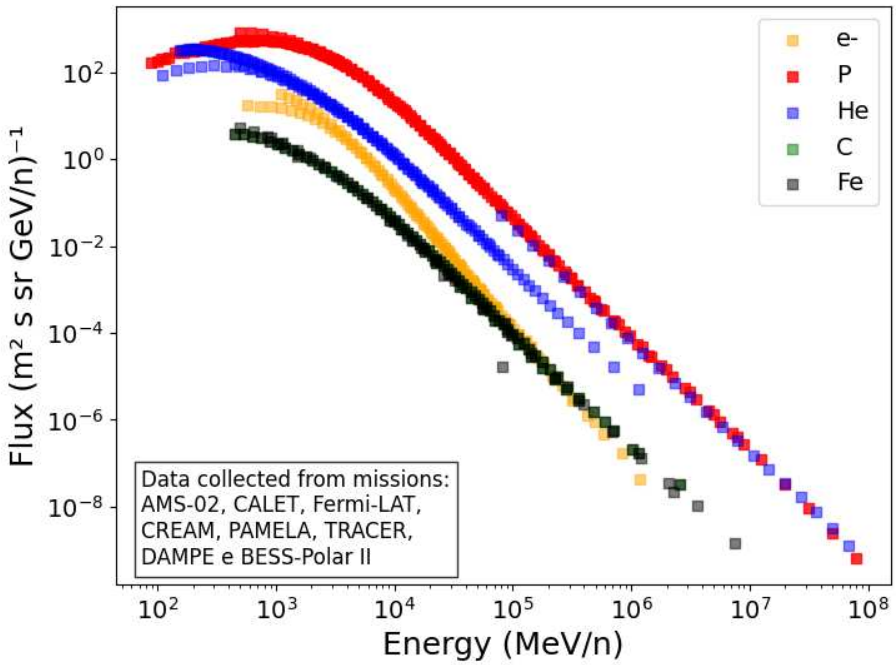

Figure 1. Primary CR spectra considered in the simulations obtained from measurements of different space missions outside the solar system.

2.3. Geant4 Parameterizations

As previously mentioned, all simulations of cosmic radiation transport and interactions within the MC were carried out using the Geant4 toolkit. To simulate hadronic interactions, the simulations employed the QGSP_INCLXX_HP reference physics list. The QGSP package integrates the quark-gluon string model to describe nucleon and pion interactions at energies above approximately 15 GeV, followed by pre-equilibrium de-excitation of the residual nuclear fragments. For lower incident energies, the Liège intra-nuclear cascade model (INCL++) is utilized. This model has been completely redesigned for improved accuracy and simulates the cascade of interactions within a nucleus, providing a detailed description of the intra-nuclear processes. The _HP suffix denotes the High-Precision NeutronHP package, which utilizes evaluated cross-section data from the ENDF/B-VII.1 library to model neutron elastic and inelastic scattering processes below 20 MeV. Electro-

magnetic interactions involving charged particles, gamma-rays, and optical photons are simulated using G4EmStandardPhysics, the recommended module for high-energy physics applications [32]. In the simulations, 1 million events were considered for each source particle type: electrons, protons, and helium, carbon, and iron nuclei.

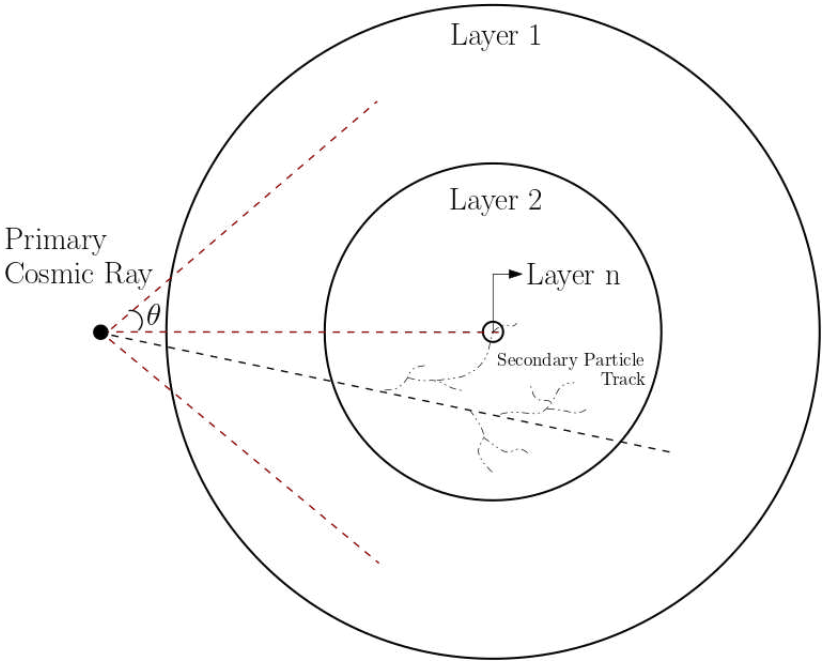

Figure 2. Schematic representation of primary galactic cosmic ray incident on the Perseus giant molecular cloud at different angles, as implemented in the Geant4 Monte Carlo simulation. The molecular cloud is modeled as a cylindrical volume aligned along the x-axis. Red dashed arrows indicate the injection directions of the primary particles. The angle θ represents the inclination of the incoming cosmic ray with respect to the cloud's longitudinal axis. This configuration enables the investigation of angular dependence in cosmic ray interactions and secondary particle production within the cloud environment. Reproduced with permission from Dr. Maurício Tizziani Pazianotto, The Astrophysical Journal; published by IOP Publishing, 2021 [20].

3. Results and Discussions

The results obtained from the Geant4 simulations offer valuable insights into the propagation behavior of cosmic ray particles within the Galaxy and their subsequent interactions with the Perseus MC. As cosmic rays penetrate the dense medium composed of gas and dust, they deposit energy along their paths, initiating a cascade of secondary particle production. These secondary particles, including gamma-rays and neutrinos, act as critical multi-messenger tracers, enabling a deeper understanding of the physical processes occurring within star-forming regions and the broader interstellar environment.

3.1. Angular Dependence of Cosmic Ray Energy Deposition in the Perseus Molecular Cloud

Understanding how cosmic ray energy deposition varies with the angle of incidence is crucial for interpreting the multi-messenger signatures of molecular clouds. Star-forming regions such as the Perseus molecular cloud act as effective targets for high-energy cosmic rays, and their layered density structure significantly modulates the propagation and interaction of incident particles. This section analyzes how the angle at which cosmic rays enter the cloud affects both the spatial and total energy deposition, key parameters for modeling gamma-ray and neutrino production.

Figure 3 presents the average energy deposited across each cloud layer for primary particles of various species, evaluated over incidence angles ranging from 1° to 80°. The re-

sults clearly show that heavy nuclei such as carbon and iron deposit significantly more energy than lighter particles like protons and electrons. This trend is expected due to the higher mass, charge, and nuclear interaction cross-section of heavier primaries, which enhance both the frequency and depth of hadronic interactions within the dense cloud material. These effects are consistent with the findings of Padovani et al. [15], who showed that high-Z cosmic ray nuclei dominate ionization and heating rates in molecular clouds due to their greater stopping power. In this context, "energy deposition" refers to the cumulative energy transferred to the cloud material by both primary and secondary particles via processes including ionization, excitation, and nuclear interactions. Geant4 computes this quantity directly by summing the localized energy losses within each layer, providing a spatially resolved profile of energy transfer rather than a simple balance of input and output energies.

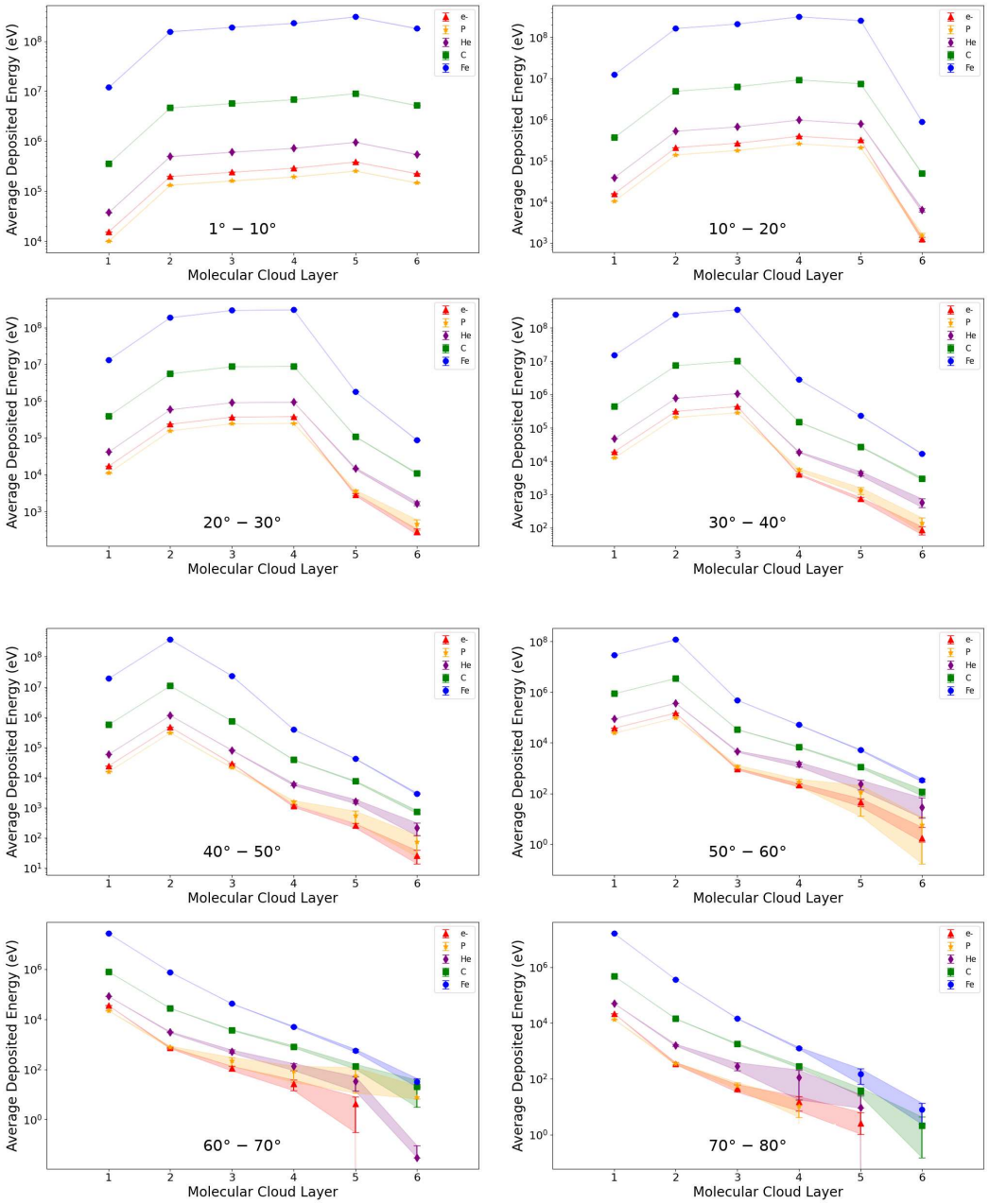

Figure 3. Average energy deposited by different cosmic ray particles as a function of the Perseus molecular cloud layer for incidence angles varying in 10-degree increments.

As the incidence angle increases, the uncertainty associated with the deposited energy gradually increases as well. Lighter primary particles, such as protons and electrons, exhibit larger error bars compared to heavier nuclei like iron. This trend can be attributed to the greater variability in the interaction cross-sections and energy deposition processes for lighter particles, especially at higher incidence angles where their interactions become less frequent and more diffuse. Similar effects have been discussed by Padovani et al. [33], who demonstrated that the propagation and attenuation of cosmic rays in dense MCs depend strongly on particle type, energy, and angle of incidence, with lighter particles being more susceptible to modulation and scattering within the cloud's complex environment. Notably, iron nuclei stand out as the only primary particles capable of depositing energy across all layers of the Perseus MC, regardless of the incidence angle. This is likely due to the higher mass and charge of iron, which results in more consistent and deeper interactions with the cloud's material, ensuring energy deposition even at grazing angles [22].

At lower incidence angles (between 1° and 10°), particles deposit energy relatively uniformly across all layers of the Perseus MC. This uniformity is due to the direct and effective interactions between the primary cosmic rays and the cloud's material, allowing energy to be transferred consistently throughout the cloud. However, as the incidence angle increases, a noticeable decrease in energy deposition occurs in the denser regions of the cloud. At higher angles, most particles are unable to penetrate deeply into these dense regions, as the cloud's chemical composition and density create a more substantial barrier to their passage. The greater the angle, the more likely the particles are to undergo scattering or absorption, limiting their ability to interact with the deeper layers of the cloud. This angular dependence is consistent with cosmic ray transport theory, which predicts that oblique incidence increases the attenuation and deflection of particles in magnetized, high-density media [15,33].

Notably, even at large incidence angles, where primary particles are expected to interact mainly within Layer 1, measurable energy deposition is observed in the deeper layers (Layers 2–6). This effect arises from the generation and subsequent propagation of secondary particles, produced during initial interactions in the outermost region. These secondaries, including neutrons, muons, and gamma-rays, can traverse significant distances and deposit energy deeper within the cloud.

Figure 4 synthesizes the total energy deposition for each particle species as a function of incidence angle. As expected, iron and carbon nuclei dominate the energy budget, with their deposition remaining high even at large angles. Protons and electrons show a decline with increasing angle, reinforcing the conclusion that heavier primaries are more efficient at transferring energy deep into dense regions, and therefore play a disproportionate role in driving hadronic cascades. Overall, these results contribute benchmark data for improving cosmic ray transport models and interpreting the angular dependence of high-energy emission from molecular clouds. This layer- and angle-resolved information can inform propagation codes, constrain models of secondary particle production, and improve estimates of the diffuse gamma-ray and neutrino backgrounds in the Galaxy.

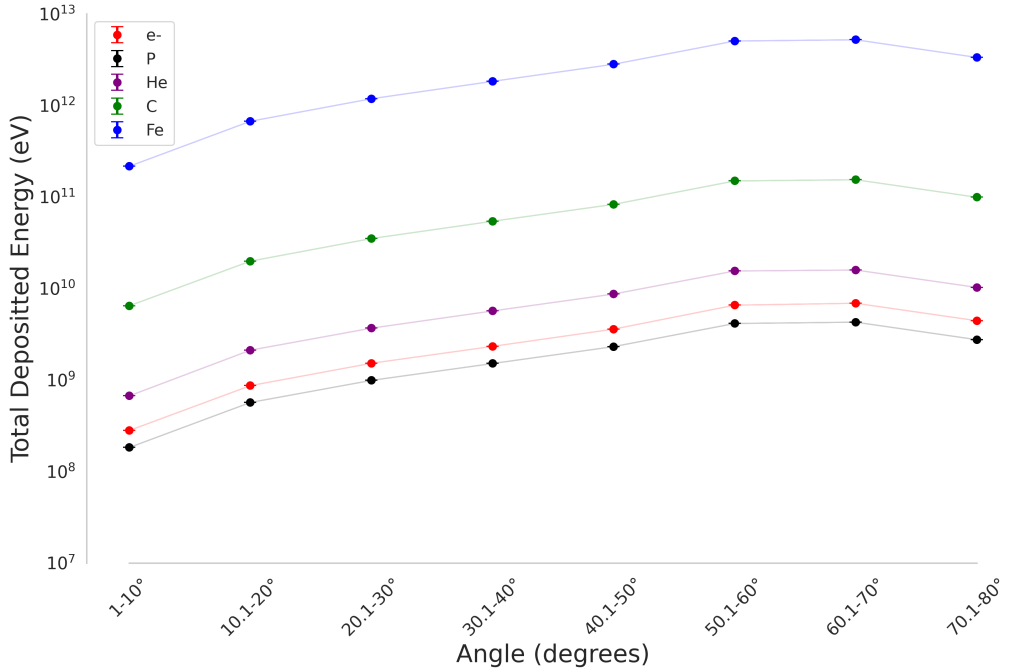

Figure 4. Total energy deposited by different cosmic ray particles as a function of incidence angles, varying in 10-degree increments, in the Perseus molecular cloud.

3.2. Emergent Secondary Particles in the Perseus Molecular Cloud

As cosmic ray particles traverse the dense medium of the Perseus molecular cloud, they continuously deposit energy along their paths. During these interactions, primary cosmic rays collide with the cloud's gas and dust, triggering the production of a variety of secondary particles. The characteristics of these secondaries are governed by both the energy of the incoming primaries and the chemical composition of the cloud. To quantify the emergent secondary spectra, we used Geant4 Monte Carlo simulations to track the interaction and propagation of primary particles through the cloud. Secondary particles were recorded as they exited the cloud, including their type, energy, and count. Their energies were binned linearly using NumPy's histogram functions, and the resulting weighted counts were normalized by the bin width to obtain differential energy spectra dN/dE, in units of particles per GeV. Statistical uncertainties were calculated from the sum of squared weights per bin and included as error bars. The final spectra are presented on logarithmic scales, highlighting the spectral shapes and intensities of the emergent particle distributions produced by different primary cosmic-ray species.

Some visible discontinuities in the secondary spectra, particularly in Figures 5–9, can be attributed to limited statistics in certain energy bins, especially for low-yield secondaries such as neutrinos, positrons, and high-energy gamma-rays. These features may appear despite small error bars, as they result from the discrete number of events contributing to sparsely populated bins. Additionally, the spectral structure is shaped by the underlying physical processes, such as pion and muon decays, which generate secondary particles with distinct energy distributions rather than smooth, power-law-like behavior.

Figure 5 illustrates the energy spectra of secondary particles, specifically electrons and gamma-rays, that originate from the interaction of primary cosmic ray electrons within the Perseus MC. In such astrophysical environments, primary electrons with relativistic energies interact with ambient gas and radiation fields, producing secondary electrons and high-energy photons through mechanisms such as bremsstrahlung, inverse Compton scattering, and knock-on (delta-ray) production [34,35]. The secondary electrons

resulting from these interactions in the Perseus region exhibit a mean energy of approximately 17.25 ± 0.08 GeV, indicative of relatively efficient energy transfer and minimal energy degradation during propagation through the cloud, which is moderately dense and rich in target protons [33]. In contrast, the associated gamma-rays, arising chiefly from bremsstrahlung and inverse Compton processes, are typically emitted with average energies of 0.90 ± 0.10 GeV, aligning with observational data from gamma-ray telescopes such as *Fermi*-LAT [36]. However, it is important to note that relativistic electrons propagating within the cloud are also subject to additional energy loss mechanisms, primarily synchrotron radiation and inverse Compton scattering, especially over spatial scales of ∼150 pc and in the presence of local magnetic fields. The magnetic field in the Perseus cloud has been estimated to be on the order of a few microgauss (μG) [25], which can lead to significant electron cooling. Although these processes are not explicitly included in the current Geant4-based simulation, which focuses on direct particle interactions and energy deposition, we acknowledge their potential impact on the final energy spectra of electrons and secondary photons. Incorporating such effects in future work will allow for a more comprehensive model of electron transport and radiation in magnetized molecular cloud environments.

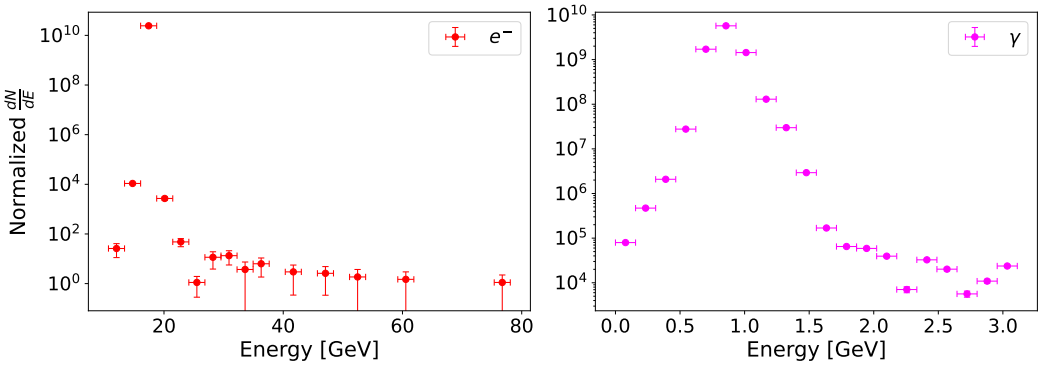

Figure 5. Spectral energy distributions of secondary particles emerging from the Perseus molecular cloud, produced by high-energy electron primaries. The red data points represent the differential energy spectrum of secondary electrons, while the magenta points correspond to gamma-rays resulting from electromagnetic interactions within the cloud.

For primary cosmic ray particles composed of hydrogen nuclei (i.e., protons, as illustrated in Figure 6), the production of secondary particles is notably more pronounced than that initiated by leptonic primaries. The baryonic charge and mass of cosmic ray protons significantly enhance the likelihood of hadronic interactions within the dense medium of the Perseus molecular cloud. These interactions primarily involve inelastic proton–proton (p-p) collisions, proceeding through the excitation and decay of baryon resonances, most notably the Δ-resonance. As a result, a substantial number of secondary particles, including charged and neutral pions ($\pi^{\pm}$, π^0), are produced [37,38]. The decay chains of these pions generate a diverse spectrum of secondary emissions: neutral pions rapidly decay into high-energy gamma-rays ($\pi^0 \rightarrow 2\gamma$), while charged pions decay into muons, which subsequently decay into electrons, positrons, and neutrinos ($\pi^{\pm} \rightarrow \mu^{\pm} \rightarrow e^{\pm} + \nu$). Additionally, secondary protons, which arise from both elastic and inelastic scattering processes, exhibit an average energy of approximately 24.20 ± 0.20 GeV, substantially higher than most other secondary species. This highlights the efficient energy transfer mechanism characterizing hadronic cascades in dense astrophysical environments [39].

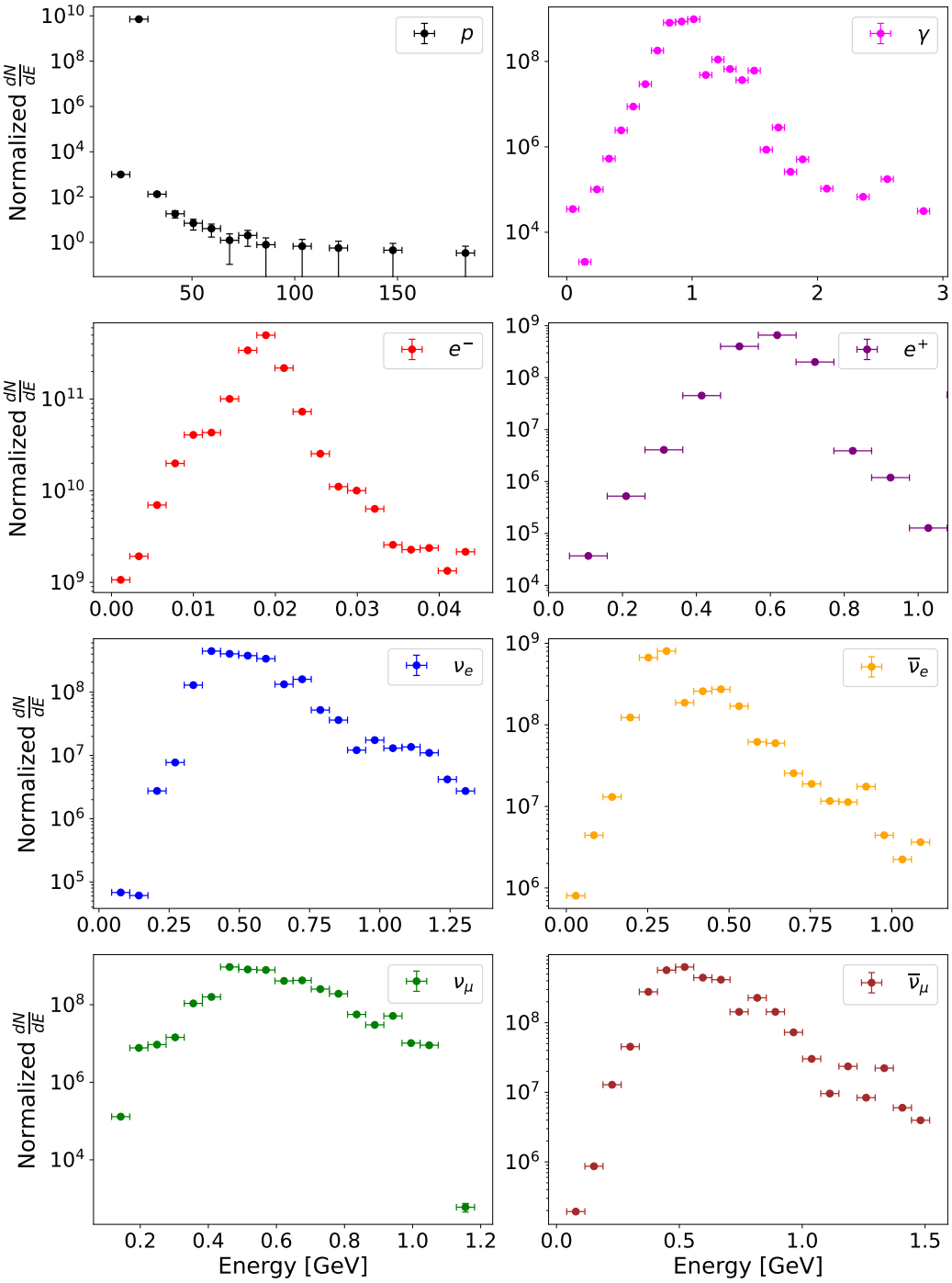

Figure 6. Spectral energy distributions of secondary particles emerging from the Perseus molecular cloud, assuming high-energy protons as the primary cosmic rays. Blue and beige data points represent electron neutrinos and antineutrinos, respectively; green and pink points correspond to muon neutrinos and antineutrinos; red and purple indicate secondary electrons and positrons; magenta shows the gamma-ray spectrum produced in the interactions; and black points represent secondary protons.

The secondary leptons and neutrinos produced through decay channels exhibit a broad range of energies. Muonic neutrinos (ν_μ) have an average energy of approximately 0.60 ± 0.10 GeV, while electronic neutrinos (ν_e) average around 0.50 ± 0.20 GeV. Electrons and positrons are generated with mean energies of 0.018 ± 0.0040 GeV and 0.60 ± 0.10 GeV, respectively. Additionally, gamma-rays originating from π^0 decay have an average energy of 0.90 ± 0.20 GeV, contributing to the diffuse high-energy gamma-ray background ob-

served in regions with active cosmic ray interactions [40]. These energy distributions align with theoretical models and observational constraints on hadronic interactions in molecular clouds, particularly those with high column densities such as Perseus. The contrast in energy retention between secondary protons and leptons underscores the nature of hadronic cascades, where nucleonic secondaries preserve a larger fraction of the primary energy. This highlights the crucial role of cosmic ray protons in shaping the multi-component spectrum of secondary particles in astrophysical environments and provides essential input for gamma-ray and neutrino production models in the interstellar medium.

Primary cosmic ray particles composed of helium nuclei (alpha particles; see Figure 7) are highly efficient in generating secondary protons with relatively high energies, averaging around 3.90 ± 0.40 GeV. Interestingly, the energy spectrum of these secondary protons closely resembles that of the associated electron neutrinos, which have mean energies near 0.240 ± 0.050 GeV. This similarity underscores their shared origin within meson decay channels resulting from inelastic nuclear interactions. As the mass of the primary nuclei increases, such as in cosmic rays composed of carbon or iron, the resulting nuclear cascades become increasingly complex, involving higher multiplicity reactions, spallation processes, and extensive meson production, particularly of charged pions ($\pi^{\pm}$). These pions undergo well-defined leptonic decay channels, initiating cascades that generate a diverse spectrum of secondary particles, including neutrinos and charged leptons [37,40]. The decay of charged pions follows the chain $\pi^+ \rightarrow \mu^+ + \nu_\mu$, $\mu^+ \rightarrow e^+ + \nu_e + \bar{\nu}_\mu$, which explains the simultaneous presence of multiple neutrino flavors and accounts for the observed positrons and electrons. These processes play a crucial role in shaping the lepton component of secondary particle populations. For helium primaries, the resulting average energies are as follows: muonic neutrinos (ν_μ) at $\sim 0.260 \pm 0.040$ GeV, electron neutrinos (ν_e) at $\sim 0.240 \pm 0.050$ GeV, positrons at $\sim 0.290 \pm 0.070$ GeV, electrons at $\sim 0.00500 \pm 0.0010$ GeV, gamma-rays at $\sim 0.280 \pm 0.060$ GeV, and protons at $\sim 3.90 \pm 0.40$ GeV.

When heavier nuclei, such as carbon, act as primary cosmic rays (see Figure 8), the resulting cascade exhibits a distinct shift. Muonic neutrinos emerge with average energies of $\sim 0.180 \pm 0.020$ GeV, electron neutrinos at $\sim 0.130 \pm 0.020$ GeV, positrons at $\sim 0.180 \pm 0.020$ GeV, electrons at $\sim 0.000790 \pm 0.000090$ GeV, gamma-rays at $\sim 0.110 \pm 0.020$ GeV, and protons at $\sim 1.80 \pm 0.10$ GeV. Compared to helium primaries, this reduction in secondary particle energies reflects both the energy-per-nucleon distribution in the incident particle and increased energy losses due to multi-nucleon interactions and nuclear fragmentation [39]. For iron nuclei (see Figure 9), the heaviest primary species considered, this trend continues, with even lower secondary particle energies: muonic neutrinos at $\sim 0.30 \pm 0.30$ GeV, electron neutrinos at $\sim 0.060 \pm 0.080$ GeV, positrons at $\sim 0.10 \pm 0.10$ GeV, electrons at $\sim 0.000163 \pm 0.0000090$ GeV, gamma-rays at $\sim 0.0040 \pm 0.0030$ GeV, and protons at $\sim 0.70 \pm 0.30$ GeV. These results illustrate how heavier nuclei, despite carrying greater total energy, tend to distribute that energy across a larger number of nucleons and interaction channels, leading to a softer secondary spectrum per particle. Additionally, the presence of muon antineutrinos as prominent byproducts of positive muon decay further underscores the leptonic richness of hadronic cascades initiated by heavier cosmic ray nuclei. These findings are consistent with previous theoretical and observational studies on cosmic ray heavy-ion interactions with molecular gas [15,41].

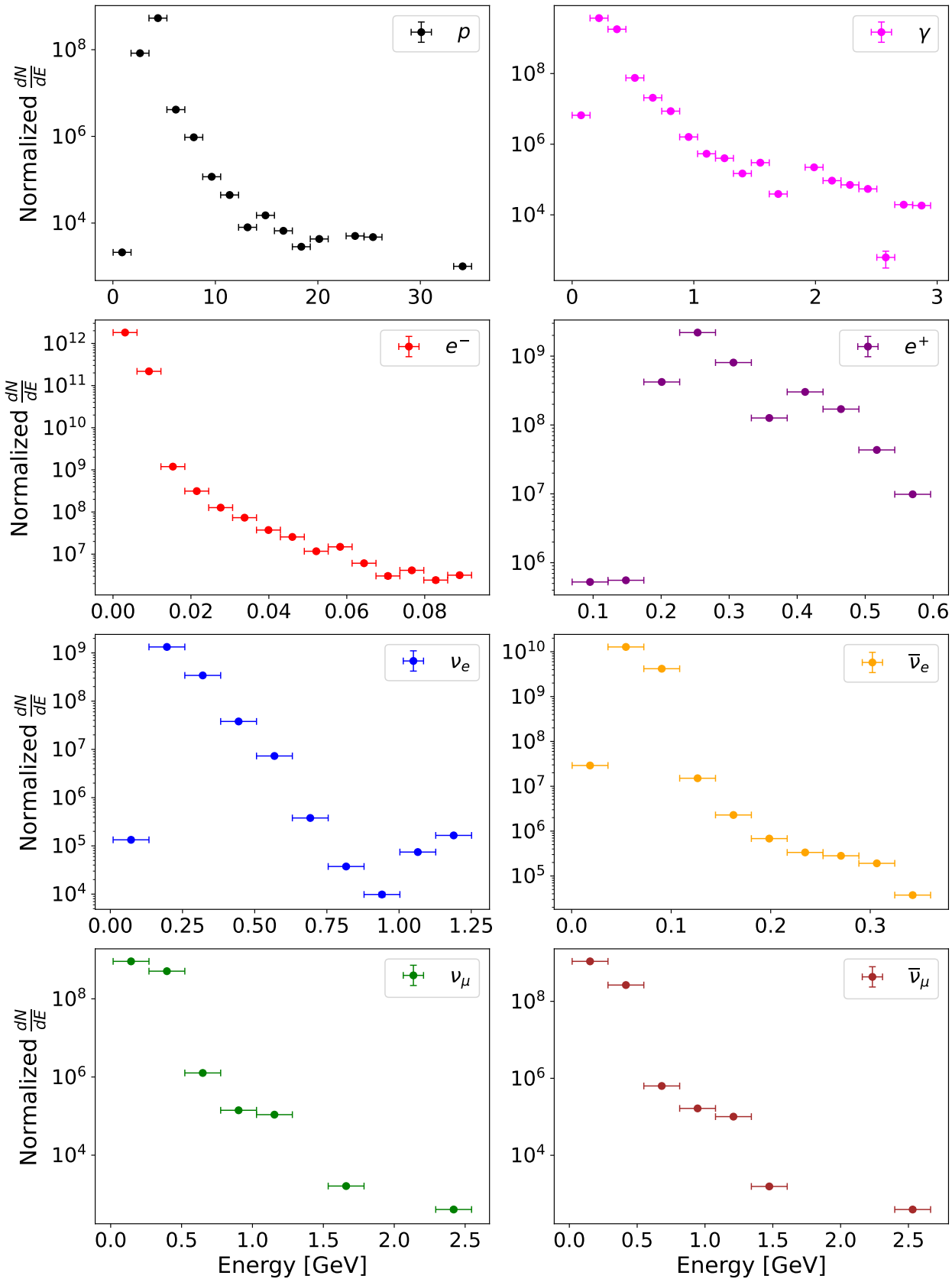

Figure 7. Spectral energy distributions of secondary particles emerging from the Perseus molecular cloud, assuming helium nuclei as the primary cosmic rays. Blue and beige data points represent electron neutrinos and antineutrinos, respectively; green and pink points correspond to muon neutrinos and antineutrinos; red and purple indicate secondary electrons and positrons; magenta shows the gamma-ray spectrum produced in the interactions; and black points represent secondary protons.

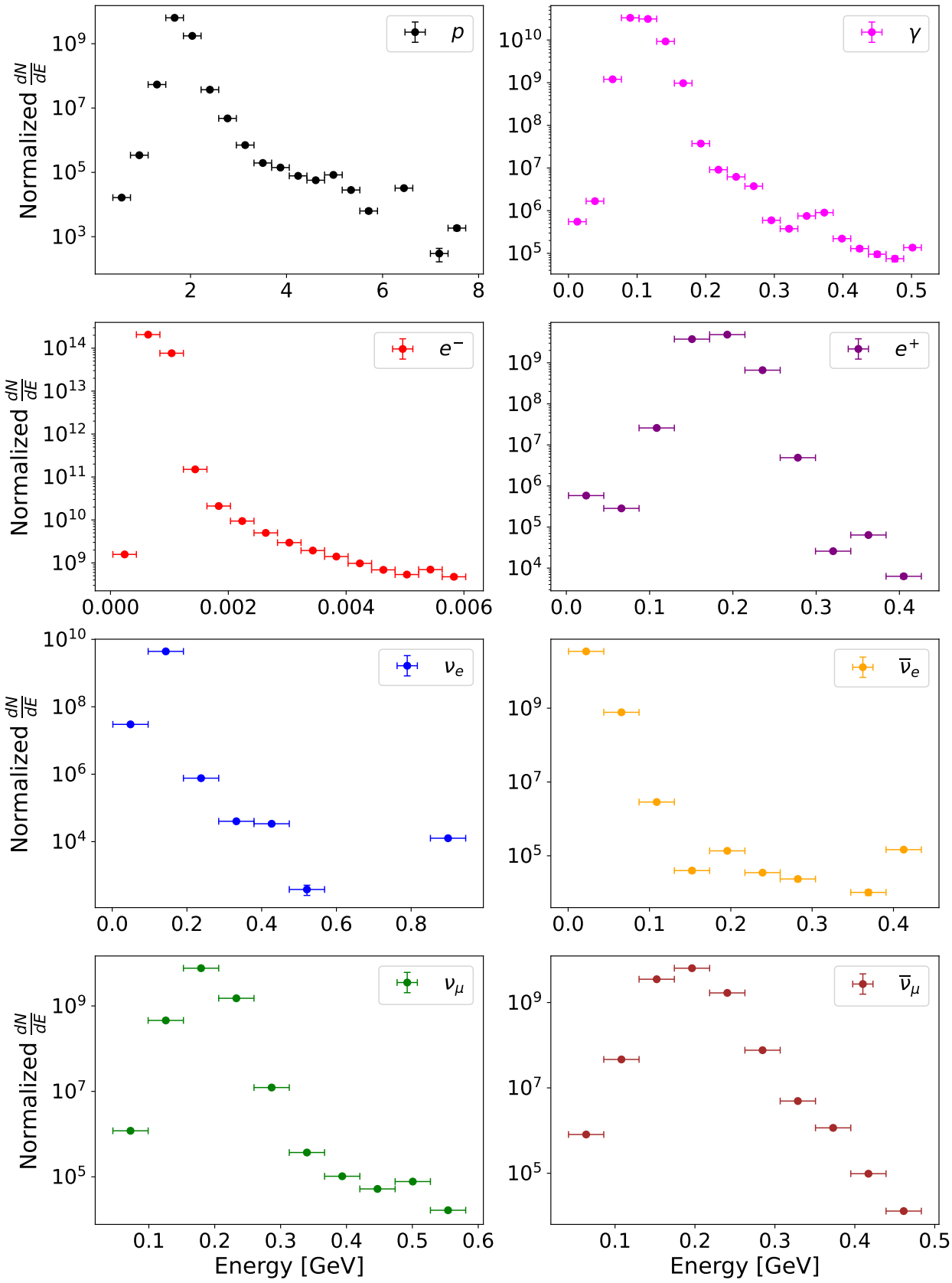

Figure 8. Spectral energy distributions of secondary particles emerging from the Perseus molecular cloud, assuming carbon nuclei as the primary cosmic rays. Blue and beige data points represent electron neutrinos and antineutrinos, respectively; green and pink points correspond to muon neutrinos and antineutrinos; red and purple indicate secondary electrons and positrons; magenta shows the gamma-ray spectrum produced in the interactions; and black points represent secondary protons.

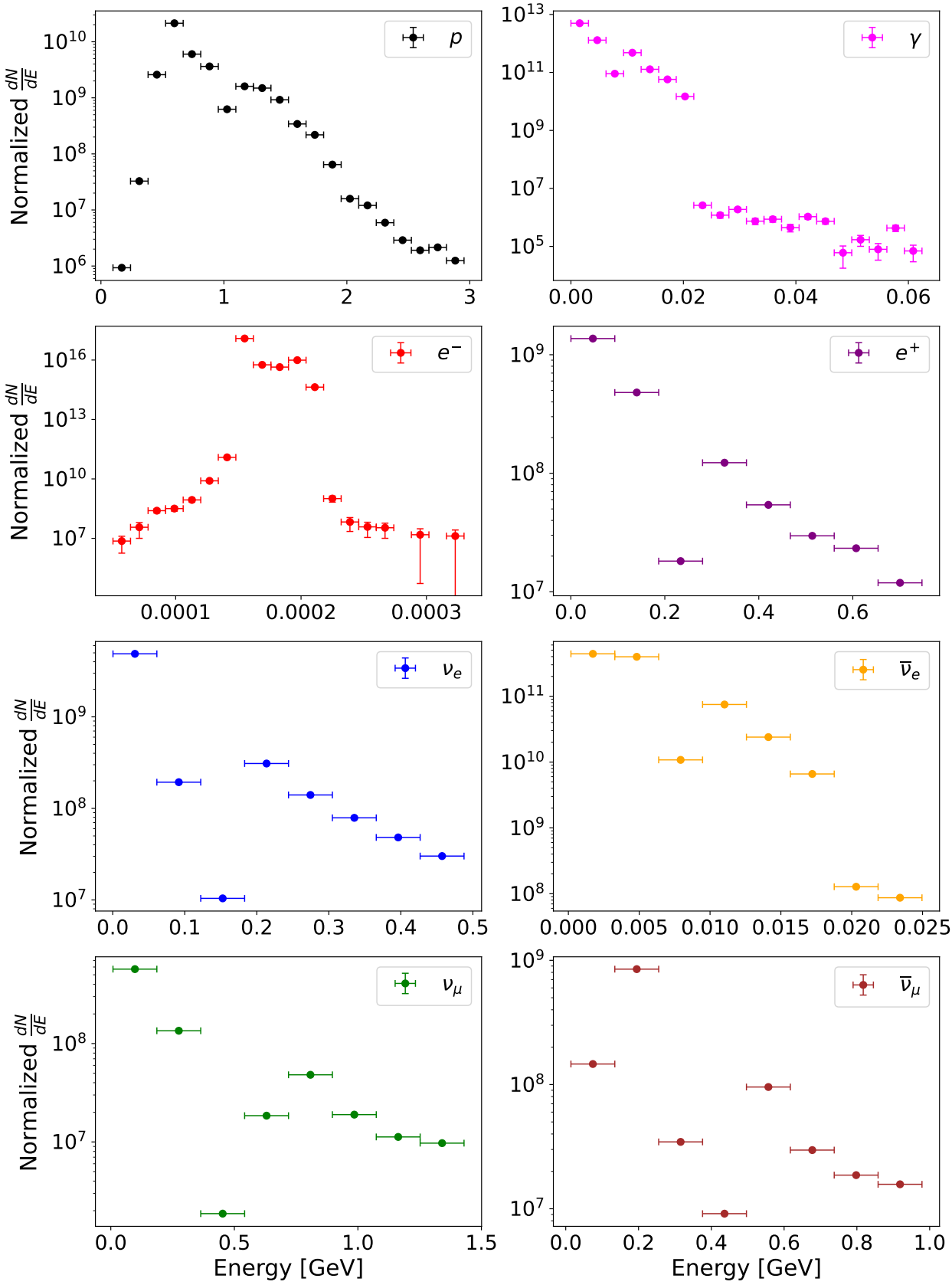

Figure 9. Spectral energy distributions of secondary particles emerging from the Perseus molecular cloud, assuming iron nuclei as the primary cosmic rays. Blue and beige data points represent electron neutrinos and antineutrinos, respectively; green and pink points correspond to muon neutrinos and antineutrinos; red and purple indicate secondary electrons and positrons; magenta shows the gamma-ray spectrum produced in the interactions; and black points represent secondary protons.

Collectively, these findings demonstrate that as the mass number of primary cosmic rays increases, the production of lower-energy secondary particles becomes more prominent, despite the rising complexity and multiplicity of interaction products. This trend plays a crucial role in understanding the contributions of various cosmic ray species to the observed high-energy neutrino and gamma-ray backgrounds in dense astrophysical environments, such as MCs. The resulting gamma-ray spectrum is strongly shaped by local cosmic ray flux, gas density, and the energy distribution of the primary particles [42–44]. Additionally, neutrino emissions serve as essential multi-messenger probes, enabling the identification and characterization of cosmic ray interaction sites within dense astrophysical regions [15,45,46].

Appendix A presents a consolidated summary of all secondary particles generated from simulations of cosmic ray interactions with the Perseus molecular cloud. The table reports the normalized abundance of each secondary particle type per 1 million primary cosmic rays, along with their corresponding average energies. This streamlined representation enables a clearer comparison across different primary species and offers a more statistically robust interpretation of the simulation results. The data provide essential context for assessing the expected secondary particle environment in molecular clouds and may serve as a useful reference for future multi-messenger observational studies.

4. Flux-Weighted Composite Spectra of Secondary Particles from Cosmic Ray Interactions

To connect our Geant4-based simulations with realistic astrophysical expectations, we computed the composite spectra of secondary particles produced by cosmic ray interactions with the Perseus giant molecular cloud, weighted by the observed fluxes of different primary species. While our simulations were carried out separately for electrons, protons, and heavier nuclei (helium, carbon, and iron), the true cosmic ray spectrum incident on the cloud comprises a mix of these species, each contributing according to its relative abundance and energy-dependent flux.

Figure 1 displays the energy spectra of primary cosmic rays used in this study, covering the range from 10 GeV to 100 TeV. To obtain a more physically meaningful prediction of the secondary particle emission from the Perseus molecular cloud, we constructed a flux-weighted combination of the individual secondary spectra produced by each primary species. The weighting factors were based on experimentally observed cosmic ray abundances, as reported by AMS-02, CREAM [47], and the CRDB [48] database. Protons, which constitute about 90% of the total cosmic ray flux at these energies, dominate the contribution. Helium nuclei follow with a relative abundance of approximately 9%. Heavier nuclei such as carbon ($\sim$0.4%) and iron ($\sim$0.04%) contribute at the sub-percent level, while electrons account for roughly 1% of the total flux [49]. This flux-weighted sum provides a more realistic estimate of the overall secondary particle spectra expected from the cloud under typical Galactic cosmic ray illumination.

The resulting composite spectra, shown in Figure 10, highlight the dominant contributions of proton and helium primaries, which account for the bulk of the cosmic ray flux. Heavier nuclei (such as carbon and iron) contribute primarily at higher energies due to their lower relative abundance but greater per-particle energy deposition. Electrons, while less abundant, still contribute notably to secondary gamma-ray production through bremsstrahlung.

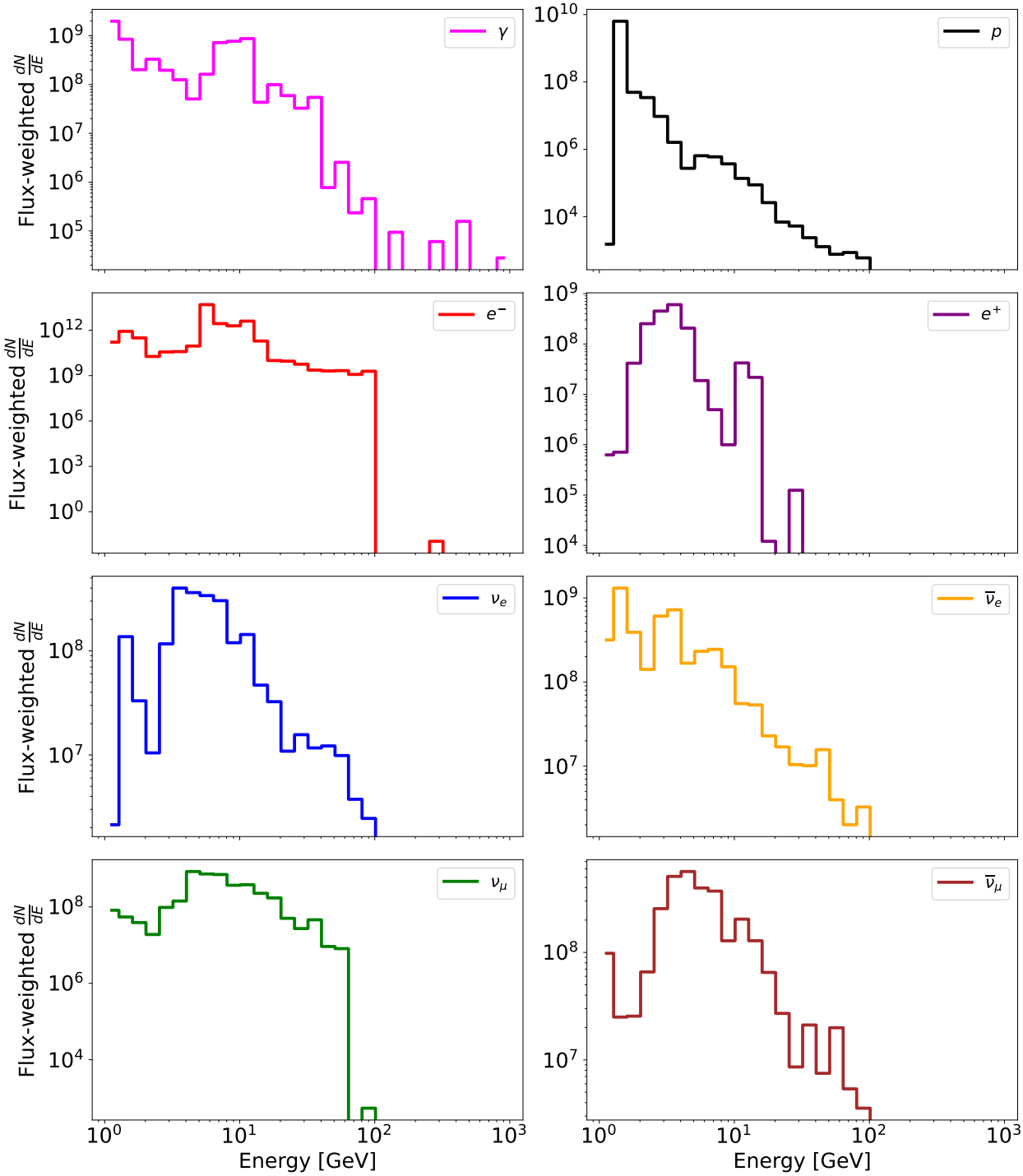

Figure 10. Spectral energy distributions of secondary particles emerging from the Perseus molecular cloud, combining contributions from all primary cosmic ray species weighted by their relative abundances. Blue and beige data points represent electron neutrinos and antineutrinos, respectively; green and pink points correspond to muon neutrinos and antineutrinos; red and purple indicate secondary electrons and positrons; magenta shows the gamma-ray spectrum produced in the interactions; and black points represent secondary protons.

By incorporating astrophysically informed flux weights, our results now provide a more observationally relevant prediction of the secondary particle environment generated by cosmic ray interactions with giant molecular clouds. This approach enhances the applicability of our simulations to future multi-messenger studies of gamma-rays, neutrinos, and other high-energy emissions from regions like Perseus.

5. Conclusions

Our Geant4 Monte Carlo simulations of galactic cosmic ray interactions with the Perseus molecular cloud provide new insights into energy deposition patterns and secondary particle production within dense astrophysical environments. We find that energy deposition varies with particle type and incidence angle, with heavier nuclei depositing more energy and exhibiting enhanced secondary particle yields. The simulations reveal that hadronic interactions, particularly from protons and heavier nuclei, are key contributors to high-energy gamma-ray and neutrino production, while electrons dominate low-energy secondary generation through ionization and bremsstrahlung.

These results highlight the critical role of molecular clouds as multi-messenger sources and demonstrate how the composition and energy of primary cosmic rays shape the resulting secondary spectra. The findings support the interpretation of molecular clouds as effective probes of cosmic ray propagation and interaction processes, and provide a robust framework for linking theoretical models with gamma-ray and neutrino observations.

Author Contributions: Conceptualization, L.A.S.P.; methodology, L.T. and L.A.S.P.; software, L.T.; validation, L.A.S.P.; formal analysis, L.A.S.P.; investigation, L.A.S.P.; resources, L.A.S.P.; data curation, L.A.S.P.; writing—original draft preparation, L.A.S.P.; writing—review and editing, L.A.S.P.; visualization, L.A.S.P.; supervision, L.A.S.P.; project administration, L.A.S.P.; funding acquisition, L.A.S.P. All authors have read and agreed to the published version of the manuscript.

Funding: Stuani Pereira, L.A. gratefully acknowledges financial support from FAPESP under grant numbers 2021/01089-1, 2024/02267-9 and 2024/14769-9, and CNPq under grant numbers 153839/2024-4 and 200164/2025-2.

Data Availability Statement: The raw data supporting the conclusions of this article will be made available by the authors on request.

Conflicts of Interest: The authors declare no conflicts of interest.

Appendix A

In this Appendix, we present a unified summary of all secondary particles produced by each type of primary cosmic ray, normalized per 1 million incident particles, that emerged from the Perseus molecular cloud.

Table A1. Normalized number of secondary particles per 1 million primary cosmic rays and their average energy. A dash (–) indicates that the secondary was not produced in the simulation.

Secondary Particle	Electron Primaries	Proton Primaries	Helium Primaries	Carbon Primaries	Iron Primaries
e^-	1.048 (2.68 GeV)	0.0509 (4.57 MeV)	0.278 (449 keV)	3.415 (93.3 keV)	47.576 (32.4 keV)
γ	0.0210 (123 MeV)	0.00166 (291 MeV)	0.00532 (57.5 MeV)	0.0450 (4.92 MeV)	0.459 (439 keV)
p	–	1.002 (4.19 GeV)	0.0120 (809 MeV)	0.0307 (324 MeV)	0.0388 (163 MeV)
e^+	–	0.00084 (285 MeV)	0.00051 (116 MeV)	0.00152 (51.4 MeV)	0.00221 (7.65 MeV)
ν_e	–	0.00084 (243 MeV)	0.00049 (144 MeV)	0.00296 (17.6 MeV)	0.0161 (1.70 MeV)
$\overline{\nu}_e$	–	0.00101 (141 MeV)	0.00457 (10.4 MeV)	0.0111 (4.78 MeV)	0.0250 (612 keV)
ν_μ	–	0.00110 (251 MeV)	0.00071 (405 MeV)	0.00055 (212 MeV)	0.00015 (182 MeV)
$\overline{\nu}_\mu$	–	0.00110 (257 MeV)	0.00071 (187 MeV)	0.00055 (192 MeV)	0.00015 (121 MeV)
deuteron	–	0.00001 (1.25 MeV)	0.00148 (2.38 MeV)	0.00202 (941 MeV)	0.00148 (710 MeV)
α	–	–	–	0.0149 (741 MeV)	0.00098 (979 MeV)
^{3}He	–	–	0.00102 (1.45 GeV)	0.00077 (2.40 GeV)	0.00019 (2.35 GeV)
triton	–	–	0.00069 (3.06 GeV)	0.00051 (884 MeV)	0.00019 (586 MeV)
^{12}C	–	–	–	0.988 (3.16 GeV)	–
^{11}B	–	–	–	0.00278 (1.72 GeV)	–
^{10}B	–	–	–	0.00122 (2.06 GeV)	–
^{6}Li	–	–	–	0.00102 (962 MeV)	–
^{7}Li	–	–	–	0.00075 (960 MeV)	–
^{9}Be	–	–	–	0.00014 (1.70 GeV)	–
^{10}Be	–	–	–	0.00003 (1.10 GeV)	–
^{13}C	–	–	–	0.00001 (31.9 MeV)	–
^{56}Fe	–	–	–	–	0.584 (4.09 GeV)
^{55}Mn	–	–	–	–	0.00219 (3.41 GeV)
^{54}Fe	–	–	–	–	0.00117 (3.97 GeV)
^{53}Mn	–	–	–	–	0.00095 (5.29 GeV)
^{52}Cr	–	–	–	–	0.00084 (4.99 GeV)
^{54}Cr	–	–	–	–	0.00065 (5.38 GeV)
^{51}V	–	–	–	–	0.00061 (6.75 GeV)
^{49}Ti	–	–	–	–	0.00023 (12.4 GeV)
^{48}Ti	–	–	–	–	0.00017 (14.4 GeV)
^{57}Fe	–	–	–	–	0.00014 (245 MeV)

The simulation framework used in this study was developed as part of a broader research project. A second manuscript is currently in preparation, which will provide a detailed description and validation of the code. To preserve the novelty and integrity of that forthcoming publication, the code is not being made publicly available at this stage. Following the publication of the second manuscript, the full code and documentation will be released in a public repository to support reproducibility and further research.

Notes

[1] https://ams02.space (accessed on 1 August 2024).
[2] https://calet.phys.lsu.edu (accessed on 1 June 2024).
[3] https://fermi.gsfc.nasa.gov (accessed on 1 August 2024).
[4] https://cosmicray.umd.edu (accessed on 1 August 2024).
[5] https://stratocat.com.ar (accessed on 1 August 2024).
[6] https://dpnc.unige.ch (accessed on 1 August 2024).

References

1. Gaisser, T.K.; Stanev, T.; Tilav, S. Cosmic Ray Energy Spectrum from Measurements of Air Showers. *Front. Phys.* **2013**, *8*, 748–758. [CrossRef]
2. Roy, A.; Joshi, J.C.; Cardillo, M.; Sarkar, R. Interpreting the GeV-TeV gamma-ray spectra of local giant molecular clouds using GEANT4 simulation. *JCAP* **2023**, *08*, 047. [CrossRef]
3. Chernyshov, D.; Caselli, P.; Cheng, K.; Dogiel, V.; Ivlev, A.; Ko, C. Interaction of cosmic rays with molecular clouds. *Nucl. Part. Phys. Proc.* **2018**, *297–299*, 80–84. [CrossRef]
4. Oka, T.; Geballe, T.R.; Goto, M.; Usuda, T.; McCall, B.J. Hot and Diffuse Clouds near the Galactic Center Probed by Metastable H_3^+. *Astrophys. J.* **2005**, *632*, 882. [CrossRef]
5. Dalgarno, A. Interstellar Chemistry Special Feature: The galactic cosmic ray ionization rate. *Proc. Natl. Acad. Sci. USA* **2006**, *103*, 12269–12273. [CrossRef]
6. Indriolo, N.; McCall, B.J. Investigating the Cosmic-Ray Ionization Rate in the Galactic Diffuse Interstellar Medium through Observations of H^+_3. *Astrophys. J.* **2012**, *745*, 91. [CrossRef]
7. Dogiel, V.; Chernyshov, D.; Kiselev, A.; Cheng, K.S. On the origin of the 6.4keV line in the Galactic Center region. *Astropart. Phys.* **2014**, *54*, 33–39. [CrossRef]
8. Dogiel, V.A.; Chernyshov, D.O.; Kiselev, A.M.; Nobukawa, M.; Cheng, K.S.; Hui, C.Y.; Ko, C.M.; Nobukawa, K.K.; Tsuru, T.G. Spectrum of Relativistic and Subrelativistic Cosmic Rays in the 100 pc Central Region. *Astrophys. J.* **2015**, *809*, 48. [CrossRef]
9. HESS Collaboration. Acceleration of petaelectronvolt protons in the Galactic Centre. *Nature* **2016**, *531*, 476. [CrossRef]
10. Aharonian, F.; Akhperjanian, A.G.; Bazer-Bachi, A.R.; Beilicke, M.; Benbow, W.; Berge, D.; Bernlöhr, K.; Boisson, C.; Bolz, O.; Borrel, V.; et al. Discovery of very-high-energy gamma-rays from the galactic centre ridge. *Nature* **2006**, *439*, 695–698. [CrossRef]
11. Yang, R.z.; de Oña Wilhelmi, E.; Aharonian, F. Probing cosmic rays in nearby giant molecular clouds with the Fermi Large Area Telescope. *Astron. Astrophys.* **2014**, *566*, A142. [CrossRef]
12. Yang, R.z.; Jones, D.I.; Aharonian, F. Fermi-LAT observations of the Sagittarius B complex. *Astron. Astrophys.* **2015**, *580*, A90. [CrossRef]
13. Tibaldo, L.; Digel, S.W.; Casandjian, J.M.; Franckowiak, A.; Grenier, I.A.; Jóhannesson, G.; Marshall, D.J.; Moskalenko, I.V.; Negro, M.; Orlando, E.; et al. Fermi-LAT Observations of High- and Intermediate-Velocity Clouds: Tracing Cosmic Rays in the Halo of the Milky Way. *Astrophys. J.* **2015**, *807*, 161. [CrossRef] [PubMed]
14. Owen, E.R.; On, A.Y.L.; Lai, S.P.; Wu, K. Observational signatures of cosmic ray interactions in molecular clouds. *Astrophys. J.* **2021**, *913*, 52. [CrossRef]
15. Padovani, M.; Galli, D.; Glassgold, A.E. Cosmic-ray ionization of molecular clouds. *Astron. Astrophys.* **2009**, *501*, 619–631. [CrossRef]
16. Zhang, Z.E.; Yang, Y.L.; Zhang, Y.; Cox, E.G.; Zeng, S.; Murillo, N.M.; Ohashi, S.; Sakai, N. The Perseus ALMA Chemistry Survey (PEACHES). II. Sulfur-bearing Species and Dust Polarization Revealing Shocked Regions in Protostars in the Perseus Molecular Cloud. *Astrophys. J.* **2023**, *946*, 113. [CrossRef]
17. Ge, H.R.; Liu, R.Y. Impact of Proton–Proton Collisions on the Cosmic-Ray Spectrum in Giant Clouds. *Universe* **2025**, *11*, 35. [CrossRef]
18. Helling, C.; Rimmer, P.B.; Rodriguez-Barrera, I.M.; Wood, K.; Robertson, G.B.; Stark, C.R. Ionisation and discharge in cloud-forming atmospheres of brown dwarfs and extrasolar planets. *Plasma Phys. Control. Fusion* **2016**, *58*, 074003. [CrossRef]

19. Padovani, M.; Galli, D. Cosmic-Ray Propagation in Molecular Clouds. In *Cosmic Rays in Star-Forming Environments*; Torres, D.F., Reimer, O., Eds.; Astrophysics and Space Science Proceedings; Springer: Berlin/Heidelberg, Germany, 2013; Volume 34, p. 61. [CrossRef]
20. Pazianotto, M.T.; Pilling, S.; Molina, J.M.Q.; Federico, C.A. Energy Deposition by Cosmic Rays in the Molecular Cloud Using GEANT4 Code and Voyager I Data. *Astrophys. J.* **2021**, *911*, 129. [CrossRef]
21. Dartnell, L.R.; Nordheim, T.A.; Patel, M.R.; Mason, J.P.; Coates, A.J.; Jones, G.H. Constraints on a potential aerial biosphere on Venus: I. Cosmic rays. *Icarus* **2015**, *257*, 396–405. [CrossRef]
22. Agostinelli, S.; Allison, J.; Amako, K.; Apostolakis, J.; Araujo, H.; Arce, P.; Asai, M.; Axen, D.; Banerjee, S.; Barrand, G.; et al. GEANT4—A Simulation Toolkit. *Nucl. Instrum. Meth. A* **2003**, *506*, 250–303. [CrossRef]
23. Allison, J.; Amako, K.; Apostolakis, J.; Araujo, H.; Dubois, P.A.; Asai, M. Geant4 developments and applications. *IEEE Trans. Nucl. Sci.* **2006**, *53*, 270. [CrossRef]
24. Toci, C.; Galli, D. Polytropic models of filamentary interstellar clouds – I. Structure and stability. *Mon. Not. R. Astron. Soc.* **2014**, *446*, 2110–2117. [CrossRef]
25. Tahani, M.; Lupypciw, W.; Glover, J.B.; Plume, R.; West, J.L.; Kothes, R.; Inutsuka, S.i.; Lee, M.Y.; Robishaw, T.; Knee, G.; et al. 3D magnetic-field morphology of the Perseus molecular cloud. *Astron. Astrophys.* **2022**, *660*, A97. [CrossRef]
26. Lee, M.Y.; Stanimirović, S.; Douglas, K.A.; Knee, L.B.G.; Di Francesco, J.; Gibson, S.J.; Begum, A.; Grcevich, J.; Heiles, C.; Korpela, E.J.; et al. A High-Resolution Study of the Hi–H2 Transition Across the Perseus Molecular Cloud. *Astrophys. J.* **2012**, *748*, 75. [CrossRef]
27. Lee, M.Y.; Stanimirović, S.; Wolfire, M.G.; Shetty, R.; Glover, S.C.O.; Molina, F.Z.; Klessen, R.S. The CO-to-H_2 Conversion Factor Across the Perseus Molecular Cloud. *Astrophys. J.* **2014**, *784*, 80. [CrossRef]
28. Bialy, S.; Sternberg, A.; Lee, M.Y.; Le Petit, F.; Roueff, E. HI-to-H2 Transitions in the Perseus Molecular Cloud. *Astrophys. J.* **2015**, *809*, 122. [CrossRef]
29. Goldsmith, P.F. Molecular Depletion and Thermal Balance in Dark Cloud Cores. *Astrophys. J.* **2001**, *557*, 736–746. [CrossRef]
30. Space Science Data Center (SSDC). *Cosmic Ray Database (CRDB)*; Space Science Data Center (SSDC): Rome, Italy, 2024.
31. Maurin, D.; Melot, F.; Taillet, R. A database of charged cosmic rays. *Astron. Astrophys.* **2014**, *569*, A32. [CrossRef]
32. Geant4 Collaboration. *Geant4 Physics Reference Manual*; Geant4 Collaboration: Geneva, Switzerland, 2023. Available online: https://geant4-userdoc.web.cern.ch/UsersGuides/PhysicsReferenceManual/ (accessed on 1 February 2025).
33. Padovani, M.; Ivlev, A.V.; Galli, D.; Caselli, P. Cosmic-ray transport in molecular clouds: The role of magnetic mirroring and focusing. *Astron. Astrophys.* **2018**, *614*, A111. [CrossRef]
34. Strong, A.W.; Moskalenko, I.V.; Ptuskin, V.S. Cosmic-ray propagation and interactions in the Galaxy. *Ann. Rev. Nucl. Part. Sci.* **2007**, *57*, 285–327. [CrossRef]
35. Kachelriess, M.; Ostapchenko, S.; Tomas, R. High energy radiation from Centaurus A. *New J. Phys.* **2009**, *11*, 065017. [CrossRef]
36. Ackermann, M.; Ajello, M.; Atwood, W.B.; Baldini, L.; Ballet, J.; Barbiellini, G.; Bastieri, D.; Bechtol, K.; Bellazzini, R.; Berenji, B.; et al. Fermi-lat observations of the diffuse γ-ray emission: Implications for cosmic rays and the interstellar medium. *Astrophys. J.* **2012**, *750*, 3. [CrossRef]
37. Gaisser, T.K. *Cosmic Rays and Particle Physics*; Cambridge University Press: Cambridge, UK, 1990.
38. Aharonian, F.A. *Very High Energy Cosmic Gamma Radiation: A Crucial Window on the Extreme Universe*; World Scientific Publishing: Singapore, 2004. [CrossRef]
39. Kachelrieß, M.; Neronov, A.; Semikoz, D.V. Signatures of a two-million year old supernova in the spectra of cosmic ray protons, antiprotons, and positrons. *Phys. Rev. Lett.* **2015**, *115*, 181103. [CrossRef] [PubMed]
40. Kelner, S.R.; Aharonian, F.A.; Bugayov, V.V. Energy spectra of gamma rays, electrons, and neutrinos produced at proton-proton interactions in the very high energy regime. *Phys. Rev. D* **2006**, *74*, 034018. [CrossRef]
41. Grenier, I.A.; Black, J.H.; Strong, A.W. The Nine Lives of Cosmic Rays in Galaxies. *Annu. Rev. Astron. Astrophys.* **2015**, *53*, 199–246. [CrossRef]
42. Aharonian, F.A.; Atoyan, A.M. Broad-band diffuse gamma ray emission of the galactic disk. *Astron. Astrophys.* **2000**, *362*, 937–952. [CrossRef]
43. Gabici, S.; Aharonian, F.; Blasi, P. Gamma rays from molecular clouds. *Astrophys. Space Sci.* **2007**, *309*, 365–371. [CrossRef]
44. Dermer, C.D. Secondary production of neutral pi-mesons and the diffuse galactic gamma radiation. *Astron. Astrophys.* **1986**, *157*, 223–229.
45. Ahlers, M.; Halzen, F. Opening a new window onto the universe with IceCube. *Prog. Part. Nucl. Phys.* **2018**, *102*, 73–88. [CrossRef]
46. Gabici, S.; Evoli, C.; Gaggero, D.; Lipari, P.; Morlino, G.; Ullio, P. The origin of galactic cosmic rays: Challenges to the standard paradigm. *Int. J. Mod. Phys. D* **2019**, *28*, 1930022. [CrossRef]
47. Yoon, Y.S.; Ahn, H.S.; Allison, P.S.; Bagliesi, M.G.; Beatty, J.J.; Bigongiari, G.; Boyle, P.J.; Childers, J.T.; Conklin, N.B.; Coutu, S.; et al. Cosmic-ray proton and helium spectra from the first cream flight. *Astrophys. J.* **2011**, *728*, 122. [CrossRef]

48. Maurin, D.; Ahlers, M.; Dembinski, H.; Haungs, A.; Mangeard, P.-S.; Melot, F.; Mertsch, P.; Wochele, D.; Wochele, J. A cosmic-ray database update: CRDB v4.1. *Eur. Phys. J. C* **2023**, *83*, 971. [CrossRef]
49. Aguilar, M.; Cavasonza, L.A.; Alpat, B.; Ambrosi, G.; Arruda, L.; Attig, N.; Azzarello, P.; Bachlechner, A.; Barao, F. Towards Understanding the Origin of Cosmic-Ray Electrons. *Phys. Rev. Lett.* **2019**, *122*, 101101. [CrossRef] [PubMed]